

Neuronal dynamics of *C. Elegans*: From calcium traces to Lyapunov spectrum

Philippe Gigon
Supervisor: Antonio Carlos Costa
ENS

January 30, 2023

Abstract

For the first time to our knowledge, the Lyapunov spectrum associated to the neuronal activity of *C. Elegans* is computed. Tools from state space reconstruction are used to embed calcium imaging time series and extract geometrical and dynamical properties of the system. The results indicate the presence of a low dimensional attractor to which the dynamics are bound. The Lyapunov spectrum admits two positive, one zero and multiple negative exponents with an overall negative dissipation rate. Comparison with previous findings on behavioural data show a similarity in the Lyapunov spectrum. This similarity indicates a direct link between neuronal activity and behaviour in *C. Elegans*.

1 Introduction

Since its dawn, neuroscience tries to understand the link between neural activity and behaviour. How is the behaviour encoded in the brain? How do complex computations take place in the brain? The brain consists of a large number of neurons which form so called neuronal networks. Those networks are aggregations of hundreds of neurons operating together. As soon as the neurons act in those networks, their dynamics become incredible complex and new properties emerge. This emergence (also known under the catchy "more is different") is at the core of statistical physics: even though we have a relatively good understanding of fundamental principles, many systems become incredibly hard to deal with as soon as a large number of those simple systems interact. Those similarities between physics and neuroscience led many physicists to study the brain. This interdisciplinary approach is indeed very promising and can shed new light on fundamental problems of neuroscience.

Experimental studies of neuronal superstructures are rather recent as they require imaging techniques which can monitor large parts of the brain simultaneously and with single cell resolution as well as advanced data treatment methods to analyse the huge amount of resulting data [1, 2]. One of those imaging techniques is given by calcium imaging, which allows to efficiently measure brain-wide activities in an organism. As this technique can be applied non invasively on transparent organism, *C. Elegans* is a very interesting subject for this kind of studies. Furthermore, the fact that *C. Elegans* has only 302 neurons, makes its brain comparatively simple and it is thus a good candidate to understand how the brain works. Having access to a large amount of good experimental data, it is necessary to develop the tools to study it. Previously, Kato *et al.* used principal component analysis on calcium imaging data and found that the brain activity of the different neurons is highly correlated and that the activity of different groups of neurons are evolving in a cyclical manner. That is, they found that the different neurons do not act independently but group together into different modes. By measuring the activity in free moving worms and capturing their motion at the same time, they were able to link collective activity of neurons to behavioural patterns [1]. Ahamed *et al.* followed a different approach using the behavioural data (recordings of the motion of *C. Elegans*) on which they applied sophisticated tools from state space reconstruction allowing them to obtain the associated Lyapunov spectrum [3].

In this paper, we use the tools developed in [3] but apply them on calcium imaging data of *C. Elegans* to compute the Lyapunov spectrum associated to the neuronal activity. This is the first time to our knowledge this computation is done and it can be of great interest to compare the thus obtained spectrum with the one from the behavioural data in [3]. The spectrum of Lyapunov exponents contains many important informations about the complex neuronal dynamics (entropy rate, dimension of the attractor, dissipation rate,...). At this stage of theory development, such first geometric insights are very useful and allow to further progress in the theoretical description of the brain.

As the computation of the Lyapunov spectrum from time series involves many difficult steps, namely embedding the data, estimating the Jacobian and then iteratively computing the exponents, those ideas are first studied and applied to the Lorenz system.

2 Theory

Many experiments in physics give data in the form of time series, that is to say, a set of measured quantities at different times. From this finite set of data at discrete time points, one wants to extract information about the underlying laws of physics. The time evolution of the physical state \mathbf{x} is given by:

$$\mathbf{x} \rightarrow \Psi(t', \mathbf{x}). \quad (1)$$

Where the point $\mathbf{x} = (x_1, x_2, \dots)$ is the set of variables which entirely specify the state of the system, we say that \mathbf{x} belongs to the state space. Ψ is an operator containing coupled differential equations in time and describing the flux of points in the state space. In the most general case, the operator is non linear in its arguments. The question is, how can we recover the "physics" behind the time series? I.e. how can we gain information about the form of Ψ from the observations at different times? In the following a method

called State Space Reconstruction (SSR) is presented. We then briefly present an algorithm which allows to compute the Lyapunov spectrum of a dynamical system. In this section, the following notations are used to distinguish the different spaces: A point of the actual state space is denoted \mathbf{x} (state space). Once a measurement is done, the measured quantity is denoted \mathbf{y} (observation space). Finally, if the measured quantity is embedded, it is denoted \mathbf{k} (reconstructed space).

2.1 State space reconstruction

As described above, the main goal is to obtain information about the state space, starting from a series of observations at different times. The theoretical framework for those purposes was given by Floris Takens in 1981 with Takens' theorem [4]. As Takens was considering an idealized problem in the absence of experimental noise, many papers followed which proposed more refined methods to tackle this problem [5, 6, 7, 8, 9].

2.1.1 Takens' theorem

Floris Takens initially studied the Taylor-Couette experiment and wanted to obtain information on the dynamical system by studying only the time evolution of an observable (the velocity of the liquid) at a given point. The state space \mathcal{H} of a system is given by the set of all variables necessary to uniquely determine the evolution of the system. Those quantities evolve according to coupled differential equations. For example, in the case of a point mass moving in 3D space, the state space is given by the three position coordinates and the conjugated momenta which evolve according to Hamilton's equations. A given state $\mathbf{x} \in \mathcal{H}$ at time t will evolve according to some time evolution function $\mathbf{x} \rightarrow \Psi(t, \mathbf{x}) \in \mathcal{H}$. A subset $\Lambda \subseteq \mathcal{H}$ to which all the different states tend asymptotically, i.e. $\forall \mathbf{x} \in \mathcal{H}, \lim_{t \rightarrow +\infty} \Psi(t, \mathbf{x}) \in \Lambda$, is called an attractor. The goal of Takens was to infer properties of the attractor using only a time series of some measured quantity. This time series is given by a smooth observation function $y : \mathcal{H} \rightarrow \mathbb{R}$, hence for a discrete set of N measurements one has the data set $\{y(\mathbf{x}_i)\}_{i=1}^N = \{y(\Psi(t_i, \mathbf{x}_0))\}_{i=1}^N$. Takens' delay-embedding theorem states that for y a smooth observation function and $M \subseteq \mathcal{H}$ a compact, d -dimensional manifold, $\Gamma_y : \mathcal{H} \rightarrow \mathbb{R}^{2d+1}$, defined as:

$$\Gamma_y(\mathbf{x}) = (y(\mathbf{x}), y(\Psi(t_1, \mathbf{x})), \dots, y(\Psi(t_{2d}, \mathbf{x}))) \quad (2)$$

is an embedding of M^1 . This theorem tells us, that it is possible to recover differential and dynamical informations about the attractor from a given set of observations [4].

Different authors have proposed extensions and new formulations of the theorem which take into account the presence of experimental noise [9, 10]. In the following the embedding method, called delay embedding, as well as a dimensionality reduction procedure are presented.

2.1.2 Time delay

The method of delays is one of the simplest methods to produce embeddings of a dynamical system and follows directly from Takens' paper. Starting from a one dimensional (this can easily be generated to more than one observable) time series $\{y_i\}_{i=1}^N$ which corresponds to observations at times separated by τ , one constructs the following matrix, called the lag matrix:

$$\mathbf{Y} = \begin{pmatrix} y_1 & y_2 & \cdots & y_K \\ y_2 & y_3 & \cdots & \vdots \\ \vdots & \vdots & \ddots & \vdots \\ y_{N-K+1} & \cdots & \cdots & y_N \end{pmatrix} \quad (3)$$

For the right choice of K , the rows of this matrix form a K -dimensional embedding of the underlying dynamical system. The choice of τ , the so called lag time, must be small enough that the different time features of the underlying system are captured and large enough that the different points are not too strongly correlated. A sufficient condition for the value of K is given by Takens' theorem [4, 6]. However, in practice one needs to estimate this parameter as the dimension of the attractor is unknown.

¹He actually says, that it is a generic property. This means that it is true for almost all possible observation functions y , we will see an exception in the following.

2.1.3 Principal Component Analysis (PCA)

PCA is procedure which allows to extract the most significant directions of a given data set and to reduce its dimension. Intuitively, the process identifies the main axis along which the data set varies the most. When making the change of basis which diagonalizes the covariance matrix, the resulting eigenvectors are the directions in which the data has a large variance and zero covariance. PCA allows thus to reduce the dimension of the data by choosing the m eigenvectors with the highest variance. Figure 1 illustrates PCA on a very simple example: Sampling from a bivariate normal distribution with mean 0 and covariance matrix:

$$\Sigma = \begin{pmatrix} 1 & c \\ c & 1 \end{pmatrix}, |c| < 1. \quad (4)$$

The principal directions can be extracted by applying the above procedure on the matrix containing the tuples (x, y) sampled from the distribution. The first panel in figure 1 shows the data coming from an uncorrelated distribution, $c = 0$. The data is more or less isotropically distributed around the origin. Panel (b) shows data sampled for $c = 0.9$ and one can clearly distinguish an anisotropy in the distribution. By applying PCA, the red and blue vectors are obtained. They point in the direction of highest variation (the red vector is associated to the larger eigenvalue of the covariance matrix). In this case, reducing the dimension of the data with PCA means projecting it on the red vector.

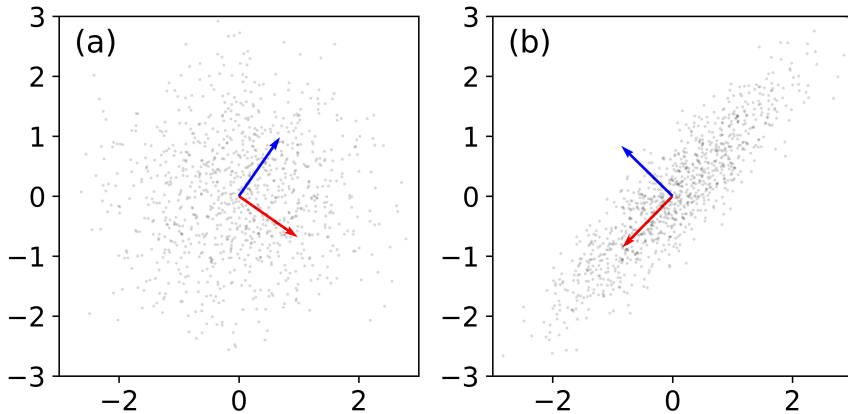


Figure 1: Illustration of PCA on a bivariate normal distribution. Panel (a) shows data sampled from an uncorrelated distribution, whereas panel (b) shows data sampled from a strongly correlated distribution. The blue and red vectors represent the two principal directions.

In the context of state space reconstruction, PCA is applied on the lag matrix \mathbf{Y} and one projects the data onto m eigenvectors associated with the largest eigenvalues. The resulting vectors form a m dimensional embedding [6]. Note that Takens' theorem gives us a sufficient condition on the embedding dimension, however it is not always necessary to embed in such high dimensions. The dimensionality reduction allows us to eliminate the additional directions. PCA furthermore maximises the signal-to-noise ratio in the presence of experimental noise.

2.1.4 Predictability

In order to embed a time series (delay embedding and dimensionality reduction) from an unknown dynamical system, one must make a choice for the parameters K (dimension of lag matrix) and m (dimension of embedding). The parameter K must be chosen in a way such that all the dynamical informations are captured by the embedding. The choice of the embedding dimension m is important as the number of Lyapunov exponents depends on the dimension of the embedding, hence one should choose m which corresponds to the actual dimension of the state space. One possible approach to choose the optimal values uses the notion of predictability, which is the capacity to forecast the evolution of the time series by looking at points in the reconstructed state space [3, 11]. In order to quantify the predictability of a system, one picks a point in the reconstructed state space, looks for close neighbours of it and then averages over their evolved state at a

later time. Figure 2a shows how the prediction is effectuated: One first finds the N_p (this parameter must be estimated) nearest neighbours of the initial point and then tracks their evolution in the reconstructed space. By going back to the observation space one can then predict the evolution and compare it to the data (Fig. 2b). In general, the dynamics is very well predicted for small times and then start to worsen. Intuitively: the more chaotic a system, the harder it is to predict for long times. At some point the prediction will be completely off and gives no better results than randomly guessing points on the attractor. In order to quantify this idea, we introduce the prediction error $E(\tau)$:

$$E(\tau) = \sqrt{\left\langle (y(t + \tau) - y_{\text{pred}}(t + \tau))^2 \right\rangle_t}, \quad (5)$$

where the average is taken over different initial times t and $y(t + \tau)$, $y_{\text{pred}}(t + \tau)$ are the actual value in observation space and the prediction of the state at $t' = t + \tau$, respectively. Starting from this prediction error, different approaches have been used in the literature. One could directly use the error at a fixed τ and evaluate the goodness of the embedding from it. This approach has some intrinsic arbitrariness, as the optimal choice of parameters might then depend on the value of τ . Hence, we use a more sophisticated metric, namely the prediction time T_{pred} as proposed in [3]:

$$T_{\text{pred}} = \frac{1}{e_s} \int_0^\infty (e_s - E(\tau)) d\tau, \quad (6)$$

with e_s the maximal prediction error, i.e. the error obtained by randomly sampling two points on the attractor landscape.

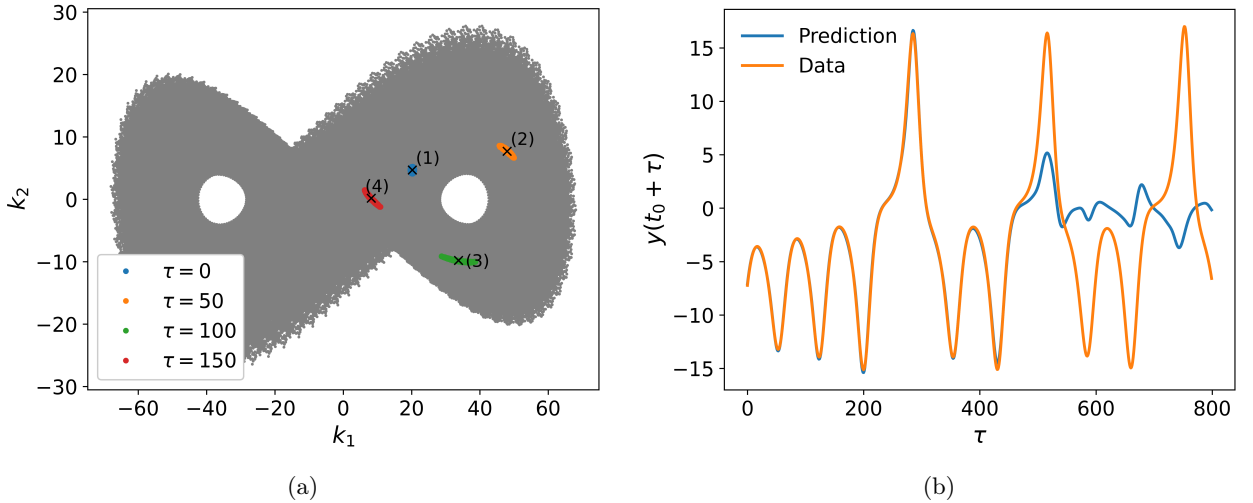


Figure 2: Illustration of the concept of predictability for Lorenz system. (a) Evolution of nearest neighbours in embedding space ($K = 25$ and $m = 3$), (b) predicted evolution of the y component in observation space.

2.2 Lyapunov spectrum

The Lyapunov spectrum is the set of all Lyapunov exponents associated to a dynamical system. This spectrum is very important as it contains information about the underlying dynamical system such as whether the system is conservative (Lyapunov exponents symmetric around zero, they sum to zero) or dissipating (sum of Lyapunov exponents negative). Therefore, it is of great interest to have an algorithm which allows to determine the Lyapunov spectrum of a given system. Starting from a hypercube in the reconstructed state space, centred at $\mathbf{k}(0)$ and spanned by some orthonormal basis vectors $\mathbf{e}_i(0)$, the i -th Lyapunov exponent λ_i is defined as:

$$\lambda_i = \lim_{t \rightarrow \infty} \log \frac{\|\mathbf{e}_i(t)\|}{\|\mathbf{e}_i(0)\|}, \quad (7)$$

where $\mathbf{e}_i(t)$ is the unit vector evolved by the dynamics in state space. Intuitively, λ_i measures the deformation of the hypercube in the corresponding direction². Locally, the dynamical system can be linearized close to the centre of the hypercube $\mathbf{k}(t)$ and a Taylor expansion gives [12]:

$$\mathbf{e}_i(t + \Delta t) \approx \exp(J(\mathbf{k}(t))\Delta t)\mathbf{e}_i(t), \quad (8)$$

where $J(\mathbf{k}(t))$ is the Jacobian of the dynamical system at point $\mathbf{k}(t)$. If the Jacobian of the system is known, the $\mathbf{e}_i(t)$ can be computed and allow to find the Lyapunov exponents. To do so, different algorithms have been proposed, here a *QR* decomposition based algorithm [12] will be used.

2.2.1 Determination of Jacobian

In order to estimate the Lyapunov exponents, the Jacobian at each point of the trajectory in the reconstructed space is needed. As the underlying differential equations are usually unknown, the Jacobian needs to be estimated from the time series data. In order to approximate the Jacobian at point $\mathbf{k}(t)$, one exploits the fact that the time evolution close to this point is determined by the Jacobian:

$$k_i(t + \Delta t) \approx \sum_{j=1}^m (1 + J_{ij}\Delta t)k_j(t), \quad (9)$$

with m the embedding dimension, and J_{ij} the coefficients of the Jacobian. Thus, with a set of neighbouring points in phase space, it is possible to estimate the coefficients of the Jacobian matrix. The implemented method was proposed by Delye *et al.* [13] and uses weighted linear regression in order to approximate the Jacobian. Starting from the time series, one weights the points according to their distance to $\mathbf{k}(t)$ and then applies linear regression to find the coefficients J_{ij} which best describe the observed dynamics. The weight w_m for each data point must be chosen in a way such that close points in phase space have a larger weight [3]. The used weight function is given by $w_m = \exp(-d_m/\varepsilon)$, where d_m is the euclidean distance between the m -th point in the time series and the point at which the Jacobian is to be estimated. ε is the average distance between two points after one period on the attractor. The quantity ε must be estimated from the available time series. The more data there is, the preciser its value can be determined. As every continuous, time-translation invariant dynamical system without fixed point on the attractor admits a zero exponent, one can do some fine tuning on this parameter in order to get the zero exponent as close as possible to zero.

2.3 Dimension of attractor

Another important property of a dynamical system with an attractor is the corresponding dimension D . The dimension of the attractor is necessarily smaller than the phase space dimension and can take fractional values. Its value is closely related to informational theoretical properties of the attractor such as its entropy. In practice it is very hard to estimate this dimension from time series data and many different definitions exist, in this article the Kaplan-Yorke as well as the correlation dimension are used [14, 15]. The first one is related to the dynamics and is computed from the Lyapunov exponents (ordered from largest to smallest):

$$D_{KY} = j + \frac{\lambda_1 + \dots + \lambda_j}{|\lambda_{j+1}|}, \quad (10)$$

where j is the largest index such that the cumulative sum $\lambda_1 + \dots + \lambda_j > 0$. The second one, the correlation dimension, is a purely geometrical property and is defined as:

$$D_c = \lim_{r \rightarrow 0} \frac{d \log C(r)}{d \log r}, \quad (11)$$

where $C(r)$ is called correlation integral and is obtained from a time series $\{\mathbf{y}_i\}_{i=1}^N$ by:

$$C(r) = \lim_{N \rightarrow \infty} \frac{1}{N^2} \sum_{i,j=1}^N \theta(r - |\mathbf{y}_i - \mathbf{y}_j|), \quad (12)$$

²This deformation can be well understood by looking at figure 2a. One can see that the nearest neighbours of the initial point (1) evolve in time and get deformed. After $\tau = 150$ steps, the evolved neighbours occupy still a connected area in the embedded space but the area is stretched in one and contracted in another direction.

θ being the Heaviside step function. The quantity $C(r)$ counts the number of points in the time series which are at most at a distance r . For small r the correlation integral behaves as a power law:

$$C(r) \sim r^{D_c}. \quad (13)$$

It is thus possible to find the correlation dimension by fitting a straight line through a loglog plot of $C(r)$ vs r .

3 Application to the Lorenz system

The Lorenz system is one of the best known examples for a system showing chaotic behaviour. It consists of the following set of coupled, first order differential equations:

$$\begin{cases} \dot{x} = \sigma(y - x) \\ \dot{y} = x(\rho - z) - y \\ \dot{z} = xy - \beta z \end{cases} \quad (14)$$

The system with $(\sigma, \rho, \beta) = (10, 28, 8/3)$ was integrated for $T = 10000$ [Δt] with time step $\Delta t = 0.01$ s and using the scipy function `integrate.odeint` starting from the initial condition $(x_0, y_0, z_0) = (-8, -8, 27)$.

3.1 Embedding

Figure 3 (a) shows the trajectory in the (x, y) plane and panels (b) and (c) are the result of a time delay embedding with matrix dimension $K = 3$ using the z and y component of the time series data. One can see that panel (c) (containing the lags of the y component) does reproduce the general topology of the attractor whereas panel (b) contains only one side of the attractor. This is a consequence of the fact that the differential equation governing the evolution of z in the Lorenz system is invariant under exchange of $(x, y, z) \rightarrow (-x, -y, z)$, therefore there are two types of trajectories which have the same dynamics along z and which lead to the folding of the attractor. Note that in practice this is not very concerning as such symmetries do not occur very often in real physical systems and if they do, even small perturbations to the variables would solve the problem (suppose there is a perturbation in the z component of the Lorenz system, in this case the symmetry would be broken). Furthermore, in a real physical experiment we would probably measure some linear combination of the coordinates x , y and z rather than one of the coordinates individually. This would also solve the problem of the symmetry in the system. Finally, panel (d) shows the complete embedding (PCA applied to the lag matrix). One can see that the geometry of the attractor is very well reproduced and it is less squeezed along the diagonal as the two principal components are uncorrelated.

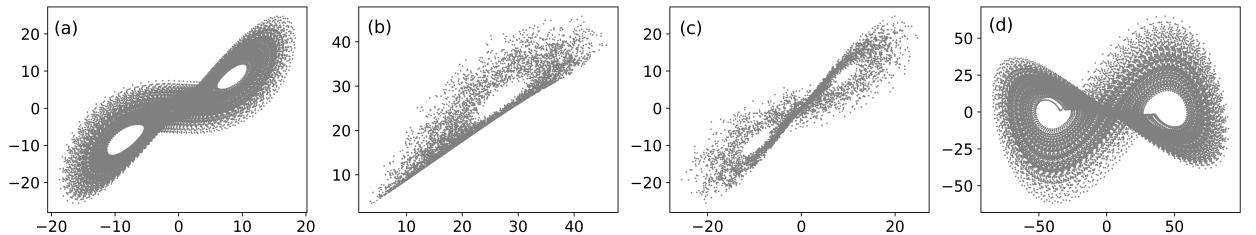


Figure 3: (a) Plot of Lorenz attractor, delay embedding (delay $\tau = 5\Delta t$) using data along z (b) and y (c), plot along two principal directions after PCA with $K = 25$ (d).

In order to test the entire data pipeline, the data along the x direction is used as time series and white gaussian noise with $\sigma = 0.005\sigma_x$ (σ_x^2 being the variance of the x component) is added. The optimal embedding parameters (K, m) have been found using the predictability time. First, the prediction time (Eq. 6) was computed for different values of the parameter K . The obtained results are shown in figure 4a. One can see

that the prediction time saturates and good results are obtained for $K = 15$, hence this value was taken for further computations. In a second step, the same procedure was repeated for fixed K and varying m . Figure 4b shows the obtained values of the prediction time. In this case the value of T_{pred} is maximal for $m = 3$ and decreases thereafter, hence for further computations m was fixed to 3. The error bars on the plots were obtained using bootstrapping and represent a 0.95 confidence interval (CI).

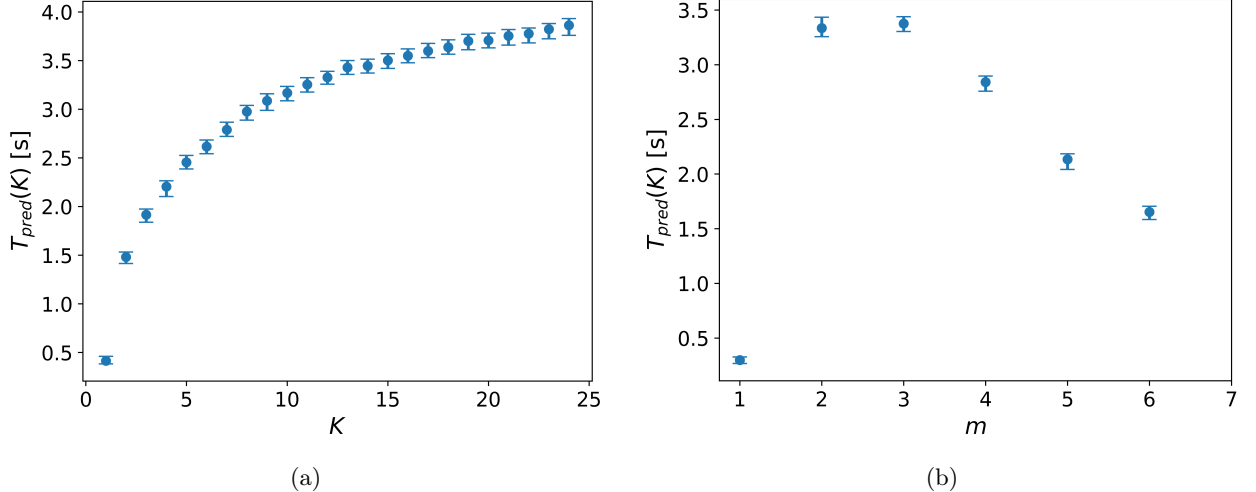


Figure 4: Prediction time obtained for different values of embedding parameter K (a) and m (b).

3.2 Computing the Lyapunov spectrum

In order to determine the Lyapunov spectrum of the Lorenz system, the above described methods have been implemented. The embedded Lorenz system was obtained by applying PCA on the lag matrix with the optimal parameters $K = 15$ and $m = 3$. As described in the theory section, the computation of the Lyapunov exponents is an iterative procedure. Therefore, it is necessary to choose a sufficient number of computation steps and to verify that the Lyapunov exponents converge to the final values. Figure 5 shows the computed values for the Lyapunov exponents at a given iteration step. One can see that the algorithm seems to converge and that the exponents only change slightly for more than 2000 steps. As there are some oscillations of the exponents even for a large number of steps, the average over the last 1000 iterations was taken.

The resulting Lyapunov spectrum is given in table 1 (Embedding with noise) together with the estimation in the case of the known Jacobian and the Jacobian estimated from all three coordinates in the observation space (Full state space).

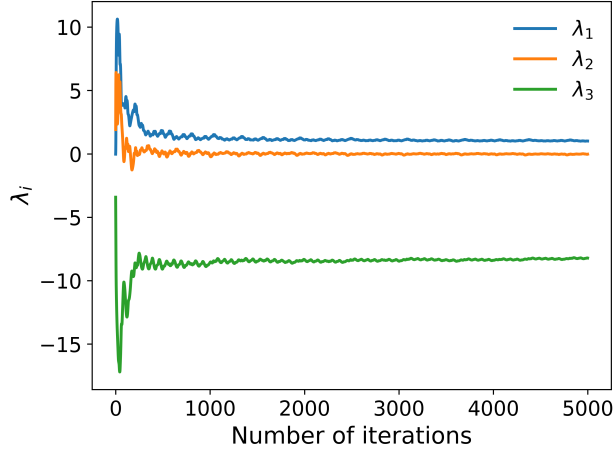


Figure 5: Convergence of the Lyapunov exponents for the embedded Lorenz system for 5000 iterations.

| | λ_1 | λ_2 | λ_3 |
|----------------------|-------------------|-------------------------------|---------------------|
| Known Jacobian | (0.90 ± 0.02) | $(-9 \pm 100) \times 10^{-5}$ | (-14.57 ± 0.05) |
| Full state space | (0.85 ± 0.04) | $(-4 \pm 10) \times 10^{-4}$ | (-9.26 ± 0.05) |
| Embedding with noise | (1.04 ± 0.03) | (-0.02 ± 0.02) | (-8.29 ± 0.04) |
| Reference [16] | 0.91 | 1.5×10^{-6} | -14.57 |

Table 1: Computed Lyapunov spectrum with known Jacobian, estimated Jacobian and from an embedding.

One can see that the reference value is very close to the results obtained with the known Jacobian. As expected, the result for the algorithm applied to the full state space is closer to the reference values than the exponents computed from the embedding. One should also note that the estimation of the smallest exponent λ_3 is the least precise. This is indeed expected as the smallest exponent is hard to capture because the dynamics in this direction are suppressed exponentially [10]. As the dynamics in this direction is very fast, one must decrease Δt in the simulation of the Lorenz system in order to better reproduce the negative exponents. I tried a $\Delta t = 0.001$ which already yielded a way better result ($\lambda_3 = -10.43 \pm 0.03$), but the corresponding code had to run for 2.5 hours. In order to correctly reproduce the smallest Lyapunov exponent, one would need to use even smaller Δt which is not possible from a computational viewpoint (on my hardware and with my algorithm which is probably not optimal).

3.3 Fractal dimension of Lorenz system

Given the embedding and the corresponding Lyapunov spectrum, one can apply the above defined formulas to find the Kaplan-Yorke and the correlation dimension of the Lorenz attractor. The computation of the Kaplan-Yorke dimension is straight forward and yields: $D_{KY} = (2.123 \pm 0.003)$. As a reference, we computed the corresponding Kaplan-Yorke dimension with the exponents coming from the known Jacobian (Tab. 1) $D_{ref} = 2.062$. The correlation dimension is obtained by computing the correlation integral and fitting the resulting curve in the linear regime. The dimension depends very strongly on the exact r regime and gives dimensions in the range $D_c \in [1.6, 2.1]$.

4 Experimental details

4.1 Calcium imaging

Neurons are behaving as electrical circuits with a potential difference between the inside and the outside of a cell, the so called membrane potential. This out of equilibrium situation is maintained by the semi-permeable cell membranes and the presence of ions such as calcium, potassium and sodium which can be transported

across the membrane through gated ion channels. When a neuron communicates with its neighbours, a so called action potential is triggered which corresponds to a rapid increase, followed by a drop in the membrane potential. This change in potential is due to the opening of the different ion channels which allow the ions to cross the membrane. Calcium imaging exploits the fact that the concentration of calcium ions is correlated to the activity in a given cell, hence by measuring the calcium concentration, one can determine the activity of the different neurons. Calcium imaging has the advantage that the brain as a whole can be analysed with single cell resolution [2]. This is done using fluorescent indicators of the calcium ions. *C. Elegans*, being a transparent organism, the imaging can be done in a non invasive manner. In order to get clean calcium imaging data, the worms are fixed. It is important to notice that this is an artificial situation and it might be reflected in the neuronal dynamics. The data used in the following corresponds to calcium traces of five different worms and comes from Kato *et al.* [1].

4.2 *Caenorhabditis elegans*

Caenorhabditis elegans, or more concisely *C. elegans*, is a nematode which has been studied for a long time in different domains of biology. This organism is known for its particularly simple brain structure consisting of only 302 identifiable neurons [1]. Some of the most important neurons used in this article are resumed in table 2.

| Neuron | Function |
|------------------------|-------------------------------------|
| RMED and RMER and RMEL | Head muscles control |
| AIBR and AIBL | Interneurons |
| RID | Unknown |
| ALA | Inhibits locomotion |
| AVBL | Driver cell for forward locomotion |
| VB01 and VB02 | Forward locomotion |
| RIMR and RIML | Modulates reversals, inhibits AVB |
| AVAR and AVAL | Driver cell for backward locomotion |
| AVER | Driver cell for backward locomotion |

Table 2: Some important neurons included into the analysis and their function [17].

5 Application to *C. Elegans*

The above described methods which have been successfully tested on the Lorenz system, are in the following applied to calcium imaging data of five subjects of *C. Elegans*. As the experimental data contains noise, additional preprocessing was applied to the data.

5.1 Preprocessing

The initial data consists of the calcium activity data of the worms. For each worm, around 110 individual neurons are labelled and their calcium imaging data is available. As the state space can be reconstructed from any number of neurons, only the 15 neurons which have been unambiguously identified across the worms, are picked for the further analysis. Hence, the initial time series is 15-dimensional. For each worm and each neuron, there is a calcium trace as the one shown in figure 6a. The y axis corresponds to the measured activity in the corresponding neuron. In order to smoothen the data a Savitzky-Golay filter is applied to it. Then, the time series are interpolated to have the same sampling rate over all the different worms. Finally, PCA was applied on the data in order to get rid of noise. Projecting to the five first principal components captures roughly 90% of the sample variance. Note that those manipulations are allowed as Takens' theorem is a statement for a generic, smooth function, hence we can apply (almost) any transformation on the data as long as it is continuous. Figure 6b shows the activity of each neuron for the first two principal components. The first component captures 75% of the sample variance and is by far the most important one. The second accounts for only 6% of the total variance.

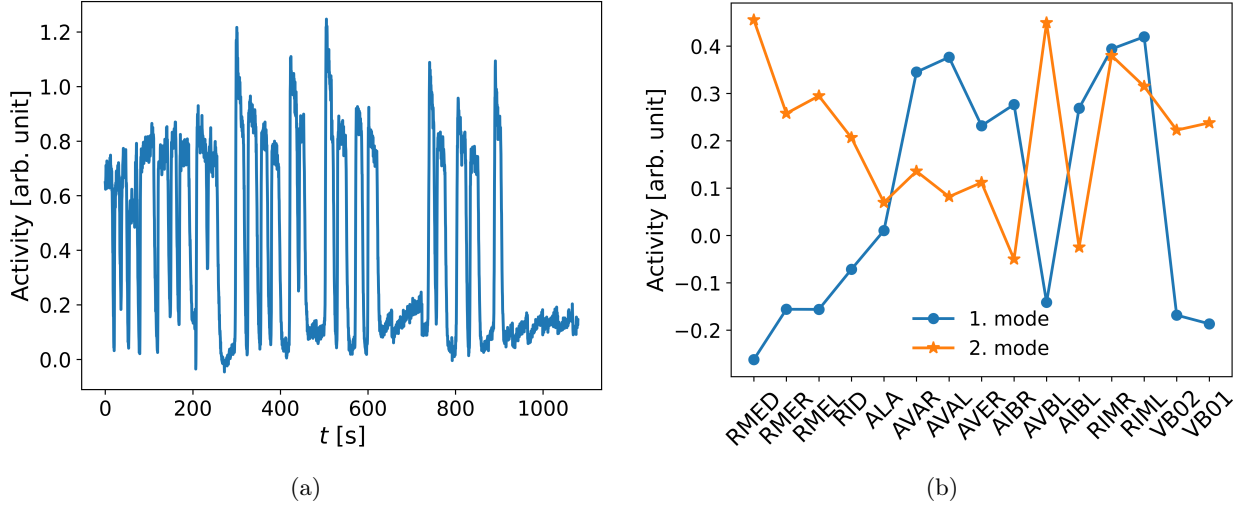


Figure 6: (a) Calcium trace of the AVAR neuron sampled from one of the worms. (b) Activity of first two PC modes for each neuron.

Figure 7 shows the first two modes with the neurons sorted according to their functionality. The first neuron, called ALA, is a neuron which inhibits motion. It is in particular active during the lethargus periods of the worm which corresponds to some sort of sleeping. The next category with three neurons in it is associated to forward motion whereas the last category contains neurons which are relevant for backwards motion. The first mode (Fig. 7a), which is also the one associated to the highest variance, is probably associated to backwards motion as the inhibitory neuron is nearly inactive and the forward neurons are anti-correlated to the backwards motion. It is very tempting to interpret this as a fleeing motion of the trapped worm. However, the next mode (Fig. 7b) reminds us to be careful with such interpretations. This mode seems to have at the same time forward and backward neurons activated. There could be multiple reasons for this:

1. This mode has way less variance than the first one (only 6%), hence it could be associated to noise.
2. It could also be associated to a more complex motional pattern such as some sort of winding which involves backwards and forwards motion at the same time.
3. Finally, it is important to remind ourselves that the simplistic view that each neuron has only one well defined function might be wrong.

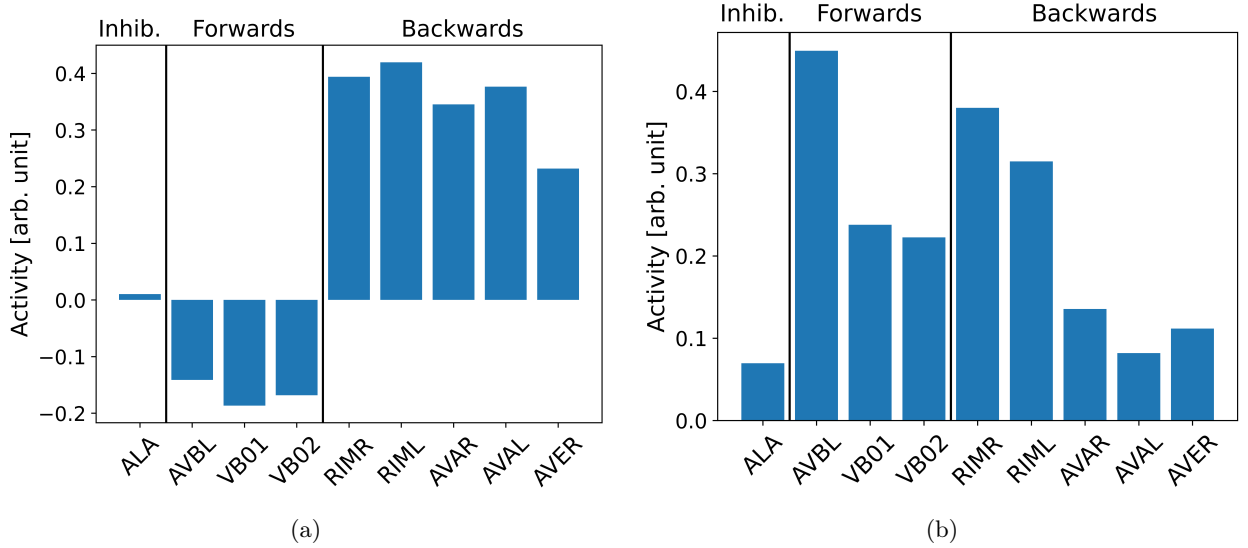


Figure 7: (a) First and (b) second mode for different neurons grouped according to their function.

5.2 Embedding parameters

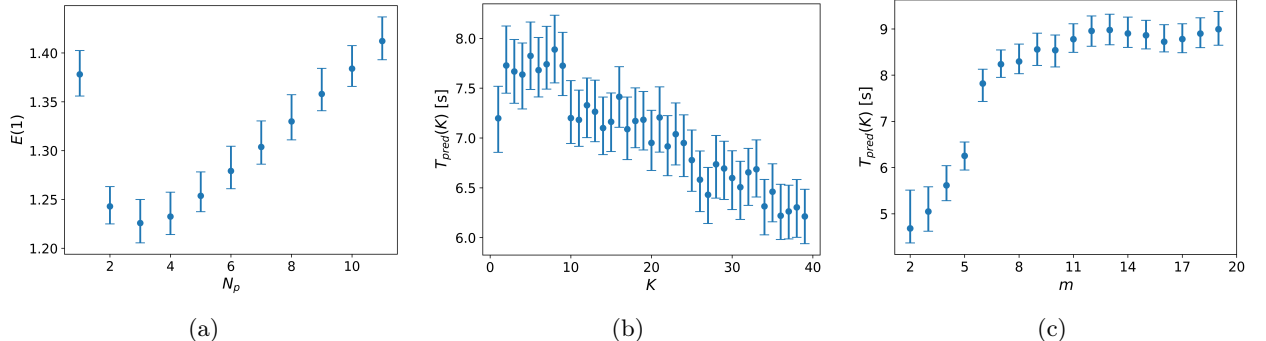


Figure 8: (a) Prediction error for a given number of nearest neighbours. Prediction time as function of (b) K and (c) m . All error bars correspond to 0.95 CI obtained by bootstrapping.

Starting from the preprocessed data, one can use the above described tools in order to determine the ideal embedding parameters. First, the one step prediction error is used in order to find the optimal value of nearest neighbours N_p . Figure 8a shows the resulting prediction errors for different number of nearest neighbours. In the following the number of nearest neighbours is fixed to $N_p = 4$. Next, the prediction time is computed for different sizes of the lag matrix. The resulting times are shown on figure 8b, therefore we use $K = 5$ and $K = 8$ (they both seem to have the same prediction time). Finally, the same procedure is repeated to find the optimal value of m using $K = 5$ (for $K = 8$ the figure is almost the same and we get the same optimal values of m), the corresponding plot is shown on figure 8c. The optimal value of m is less clear than it was for the Lorenz system, therefore the Lyapunov spectrum is computed for different values $m \in \{6, 7, 8, 9\}$. Figure 9 shows the fraction of the total variance captured for different values of the embedding parameter m . One can see that approximately 82.5% of the variance is contained in the first mode. The captured variance does strongly increase for $m < 7$ and then flattens out. From this perspective it seems reasonable to choose m in the range stated above and using higher values will most likely capture experimental noise without adding further information about the system.

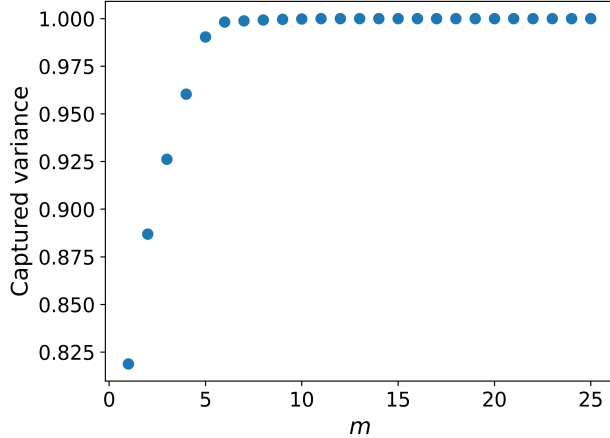


Figure 9: Fraction of captured variance of embedding as function of parameter m .

5.3 Lyapunov spectrum

Using the above found values of K and the different values of m , we can compute the Lyapunov spectrum associated to the embedding. For each worm the Lyapunov exponent is computed and averaged over the 1000 last iterations of the algorithm, finally all the resulting exponents are averaged over the different worms. In order to fine tune the parameter ε (used to estimate the Jacobian), the zero exponents were used. The initial values of ε found by geometric considerations (average distance after one orbit), were slightly perturbed in order to minimize the absolute value of the zero exponent. The final Lyapunov spectrum with embedding parameters $K = 5$ and different values of m are shown in figure 10 with the CI given by one standard deviation. The spectra for embeddings with $K = 8$ can be found in the appendix.

As already observed with the Lorenz system, the negative Lyapunov exponents are very hard to estimate and come with a large error. It is also very interesting to notice that the number of positive exponents (two) stays the same for every value of m and that their sum is approximatively constant (see Tab. 3). If one increases the embedding dimension m , the total sum of the Lyapunov exponents becomes more negative, hence the system is more dissipative. The dimension of the attractor does strongly depend on the embedding parameters and varies a lot. This is not surprising as in the definition of the Kaplan-Yorke dimension we are dividing by the first exponent such that the cumulative sum becomes negative. This negative exponent comes with large uncertainty as seen on figure 10.

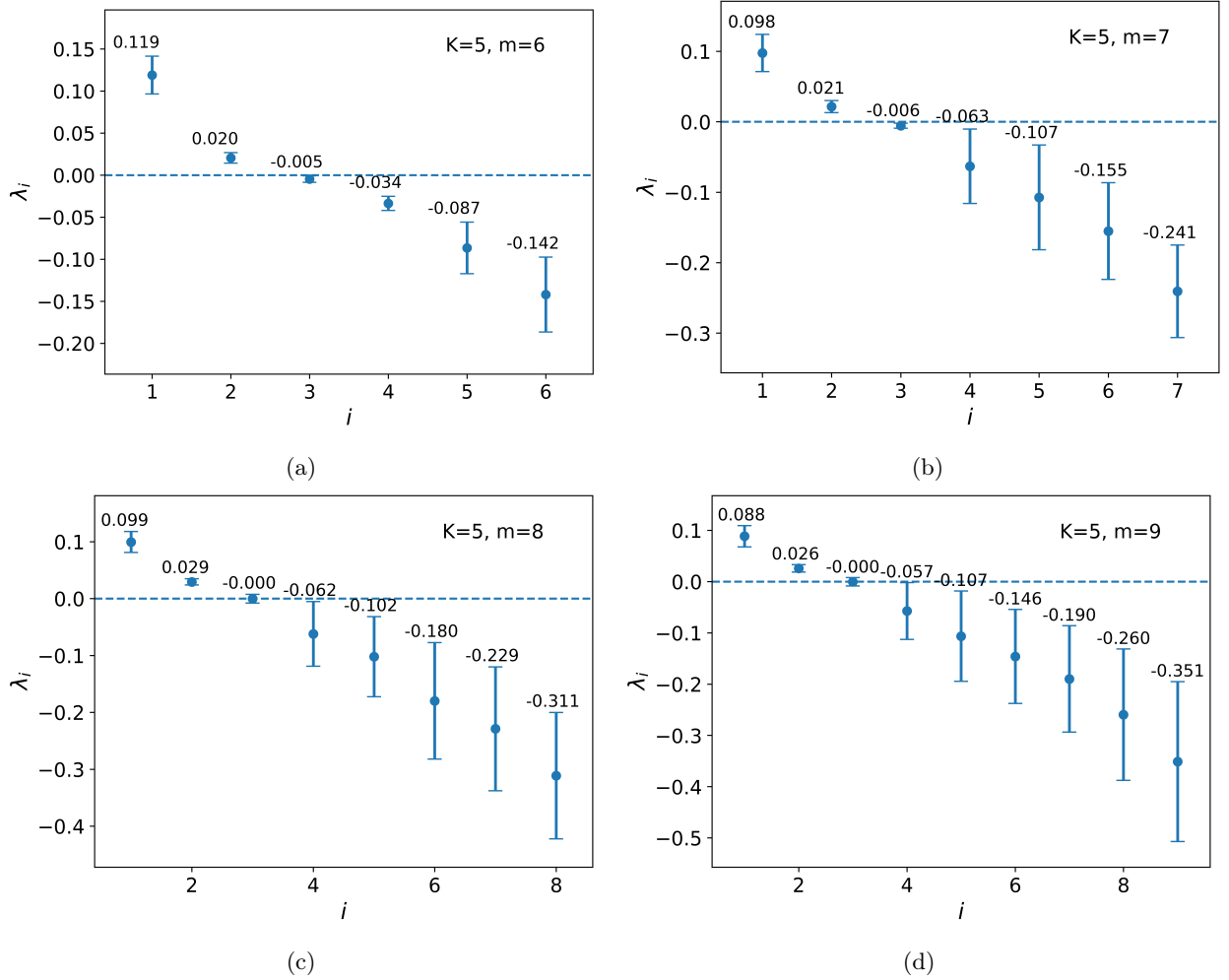


Figure 10: Lyapunov exponents computed from calcium imaging data of *C. Elegans* for $K = 5$ and $m = 6$ (a), 7 (b), 8 (c), 9 (d). The given values correspond to the computed Lyapunov exponents.

| (K, m) | $\sum_{\lambda_i > 0} \lambda_i$ | $\sum_i \lambda_i$ | $\min(\lambda_i)$ | D_{KY} |
|----------|----------------------------------|--------------------|------------------------------|-----------------|
| (5, 6) | (0.14 ± 0.03) | (-0.1 ± 0.1) | $(5 \pm 6) \times 10^{-3}$ | (5.1 ± 0.7) |
| (5, 7) | (0.12 ± 0.03) | (-0.5 ± 0.3) | $(6 \pm 3) \times 10^{-3}$ | (4.5 ± 0.8) |
| (5, 8) | (0.13 ± 0.02) | (-0.8 ± 0.5) | $(3 \pm 70) \times 10^{-4}$ | (4.6 ± 0.9) |
| (5, 9) | (0.11 ± 0.03) | (-1.0 ± 0.7) | $(5 \pm 700) \times 10^{-4}$ | (4.5 ± 0.9) |
| (8, 6) | (0.15 ± 0.03) | (-0.1 ± 0.1) | $(2 \pm 4) \times 10^{-3}$ | (5.3 ± 0.7) |
| (8, 7) | (0.13 ± 0.03) | (-0.3 ± 0.2) | $(2 \pm 70) \times 10^{-4}$ | (5.2 ± 1.0) |
| (8, 8) | (0.13 ± 0.02) | (-0.4 ± 0.3) | $(6 \pm 800) \times 10^{-5}$ | (9.1 ± 1.2) |
| (8, 9) | (0.15 ± 0.03) | (-0.7 ± 0.5) | $(1 \pm 10) \times 10^{-3}$ | (8.5 ± 1.9) |

Table 3: Dynamical properties of the attractor computed for different embedding parameters K and m . The errors correspond to one standard deviation over the last 1000 iterations of the corresponding Lyapunov exponent. Note that the errors for the zero exponent seem to be very big, however this is not surprising as they are all very close to zero.

6 Discussion

6.1 Application to Lorenz system

The implemented algorithms have been tested with the well-known Lorenz system and the resulting Lyapunov exponents are given in table 1. The computed Lyapunov spectrum for known Jacobian matches very well the reference values given in [16]. The embedding of the data was then done by constructing the lag matrix followed by dimensionality reduction with PCA and the optimal parameters were estimated using the prediction time as proposed in [3]. The optimal value of $K = 15$ was chosen as the prediction time only increases slightly for larger values. $m = 3$ was chosen as the prediction time starts to decrease again for $m > 3$. The fact that the prediction time starts to decrease for larger values is due to the added noise. Indeed, if one doesn't add noise to the data, the prediction time saturates for larger values of m whereas in the case with noise, the additional PCA modes are mainly due to noise (low variance modes) and hence the prediction time worsens.

This embedding allowed to find the Lyapunov spectrum. The largest and the zero exponent are consistent with the reference value, the smallest exponent is estimated less precisely. This result is in fact not surprising as negative exponents are very hard to estimate. Indeed, as the corresponding dynamics are suppressed very quickly, one must use data points which are more closely spaced (hence smaller Δt). As the algorithm takes a lot of time to run, it was not possible to decrease Δt any further than 0.001. Besides this, one can conclude that the computation of the Lyapunov spectrum from an embedding works well for positive and zero exponents and that the most negative exponents must be treated carefully.

Finally, the fractal dimension of the attractor was computed. The Kaplan-Yorke dimension is straight forward to compute when the Lyapunov spectrum is given, however its precision depends on the precision of the Lyapunov spectrum. The obtained value is reasonably close to what is obtained from the Lyapunov spectrum with known Jacobian D_{ref} . The correlation dimension is way harder to compute and the result depends strongly on the regime where one makes the fit. Depending on the r regime where the correlation dimension was computed, the resulting dimension is somewhere in the interval [1.6, 2.1], which is the right order of magnitude, but not precise enough to extract interesting information. There might indeed be a problem with my computations, hence I decided not to pursue this approach for *C. Elegans*.

6.2 Neurons of *C. Elegans*

The fact that there are only few neurons in the nervous system of *C. Elegans* makes it comparatively simple to identify the different functions of each neuron. This particularity is very interesting as it allows to make a link between the well known function of each neuron and the infinitely more complex collective behaviours. Indeed, the analysis of single neurons in *C. elegans* may shed light on how more complex behaviour can emerge. It is therefore very interesting to see how the different modes found from the data seem to correspond to what one would expect intuitively: The first PCA mode given in figure 7a is characterised by the joint action of neurons associated to backward motion whereas the ones associated to forward motion are anti-correlated. This finding does in fact well match with the results of Kato *et al.* [1]. They applied PCA on the time derivatives of the calcium traces and found very similar PCA modes, namely they have the same qualitative behaviour for the first mode.

6.3 Lyapunov spectrum

Using the embedding method first tested on the Lorenz system, the calcium imaging data of the neuronal activity of *C. Elegans* was embedded. The optimal number of nearest neighbours was determined and the lag parameter K was obtained using prediction time. Two values with the same predictability time have been used ($K = 5$ and $K = 8$). In the case of the parameter m , no obvious optimal value has been found, hence the embedding was done for different embedding dimensions ($m \in \{6, 7, 8, 9\}$). At first sight this seems to be problematic as the number of Lyapunov exponents changes with the embedding dimensions, but the computations have shown that the number of positive exponents is the same (two positive exponents) for all the different dimensions (Fig. 10). This indicates a certain degree of robustness as one would expect from

Takens' theorem. If even higher values of m are included ($m > 9$) in the analysis the qualitative behaviour of the spectrum seems to change and the exponents become more negative. But as figure 9 shows that every mode with $m > 6$ captures only very little variance (and are most likely due to experimental noise) I decided to exclude the higher embedding dimensions from the analysis. At this point it should be pointed out that the obtained results are to be taken with a grain of salt: The data contains experimental noise and the computed exponents come with a large uncertainty. This issue could easily be removed by applying the same treatment to more data (allowing to observe over multiple oscillations).

Having that said, the computed Lyapunov spectrum shows very interesting properties, namely the sum of positive exponents remains almost constant for different embedding dimension and different values of K . This observation is reassuring as the sum of the positive exponents is a measure for the chaotic behaviour of the system (it is equal the Kolmogorov-Sinai entropy per unit time [18]). When one adds more dimensions, they are associated to negative Lyapunov exponents and the corresponding directions are thus suppressed exponentially. One should also note that the total sum of the Lyapunov exponents is negative (dissipative system). The presence of an almost zero exponent is indicating chaotic behaviour with very long timescales ($\tau = 1/\lambda$). From a biological perspective, one might be tempted to speculate that this long time scale behaviour is linked to slower biological processes such as long term adaptation in the synapses or long term behavioural patterns (searching for food?). The Kaplan-Yorke dimension yields values between 4.5 ± 0.9 and 9.1 ± 1.2 . As the negative Lyapunov exponents come with a large variance, it is not surprising that the Kaplan-Yorke dimension varies a lot, however an attractor dimension of $D_{KY} \approx 5$ seems reasonable. This dimension is in fact close to the dimension of the embedding space, hence the dynamics still visit a large part of the embedding space.

Finally, it is very interesting to link our results with the findings of Ahamed *et al.* [3]. Having applied the exactly same tools on behavioural data of *C. Elegans*, they found an optimal embedding of dimension $m = 8$. They also found a spectrum with two positive Lyapunov exponents, and one very close to zero. Their dissipative rate is $\sum_i \lambda_i = -0.94$ which is close to our results (Tab. 3). Having access to larger amounts of high quality data, they were able to obtain more reliable results and discovered a symmetry in the Lyapunov spectrum suggesting to interpret the behavioural dynamics as a system of coupled, damped and driven Hamiltonian oscillators. Their Kaplan-Yorke dimension is $D_{KY} = 6$ which is also close to what we found. All of these similarities between the behavioural and the neuronal data are very intriguing as they make the link between behaviour and neuronal activity and should definitely be further investigated. To do so, larger amounts of neuronal data is needed allowing to have more significant results.

7 Conclusion

The methods of state space reconstruction have been successfully implemented and tested on the Lorenz system. Having at hand those tools, they were applied to calcium imaging data sampled from the nematode *C. Elegans*. The embedding allowed to estimate the Lyapunov spectrum associated to the neuronal dynamics and showed clearly chaotic behaviour. The number of Lyapunov exponents was found to be between 6 and 9 corresponding to the embedding dimension. For each embedding dimensions, two positive exponents and one zero exponent were found. The sum of the exponents indicates that the dynamics is dissipative and bound to an attractor. Comparison of the results with findings from Ahamed *et al.* shows a link between the spectrum obtained from behavioural and from neuronal data. The optimal embedding dimension they found ($m = 8$), the attractor dimension, the dissipation rate as well as the number of positive exponents are very similar to our findings. Indeed, by Takens' theorem one could have anticipated this result: If the behaviour is some smooth function of the neuronal activity, the two approaches should lead to the same Lyapunov exponents. The analogies between brain and behaviour are very intriguing and require further investigations.

In a next step it would be interesting to apply our tools to a larger and neater data set allowing to extract the spectrum with higher confidence. The resulting spectrum could than be compared in more detail to behavioural data allowing to further investigate the relations between behaviour and neuronal activity.

From an algorithmic perspective, it would be interesting to use a chaotic recurrent network to compute the Lyapunov spectrum (Engelken *et al.* [19]).

References

- [1] Saul Kato et al. “Global brain dynamics embed the motor command sequence of *Caenorhabditis elegans*”. In: *Cell* 163.3 (Oct. 2015), pp. 656–669.
- [2] Francesco Randi and Andrew M Leifer. “Measuring and modeling whole-brain neural dynamics in *Caenorhabditis elegans*”. In: *Current Opinion in Neurobiology* 65 (2020). Whole-brain interactions between neural circuits, pp. 167–175. ISSN: 0959-4388. DOI: <https://doi.org/10.1016/j.conb.2020.11.001>. URL: <https://www.sciencedirect.com/science/article/pii/S0959438820301689>.
- [3] Tosif Ahamed, Antonio C. Costa, and Greg J. Stephens. “Capturing the continuous complexity of behaviour in *Caenorhabditis elegans*”. In: *Nature Physics* 17.2 (2021), pp. 275–283. ISSN: 1745-2481. DOI: 10.1038/s41567-020-01036-8. URL: <https://doi.org/10.1038/s41567-020-01036-8>.
- [4] Floris Takens. “Detecting Strange Attractors in Turbulence”. In: *Dynamical Systems and Turbulence, Warwick 1980*. Ed. by David Rand and Lai-Sang Young. Vol. 898. Lecture Notes in Mathematics. Berlin: Springer, 1981. Chap. 21, pp. 366–381. ISBN: 978-3-540-11171-9. DOI: 10.1007/bfb0091924.
- [5] Henry D. I. Abarbanel et al. “The analysis of observed chaotic data in physical systems”. In: *Rev. Mod. Phys.* 65 (4 1993), pp. 1331–1392. DOI: 10.1103/RevModPhys.65.1331. URL: <https://link.aps.org/doi/10.1103/RevModPhys.65.1331>.
- [6] D.S. Broomhead and Gregory P. King. “Extracting qualitative dynamics from experimental data”. In: *Physica D: Nonlinear Phenomena* 20.2 (1986), pp. 217–236. ISSN: 0167-2789. DOI: [https://doi.org/10.1016/0167-2789\(86\)90031-X](https://doi.org/10.1016/0167-2789(86)90031-X). URL: <https://www.sciencedirect.com/science/article/pii/016727898690031X>.
- [7] Martin Casdagli et al. “State space reconstruction in the presence of noise”. In: *Physica D: Nonlinear Phenomena* 51.1 (1991), pp. 52–98. ISSN: 0167-2789. DOI: [https://doi.org/10.1016/0167-2789\(91\)90222-U](https://doi.org/10.1016/0167-2789(91)90222-U).
- [8] John F. Gibson et al. “An analytic approach to practical state space reconstruction”. In: *Physica D: Nonlinear Phenomena* 57.1 (1992), pp. 1–30. ISSN: 0167-2789. DOI: [https://doi.org/10.1016/0167-2789\(92\)90085-2](https://doi.org/10.1016/0167-2789(92)90085-2). URL: <https://www.sciencedirect.com/science/article/pii/0167278992900852>.
- [9] Ethan R. Deyle and George Sugihara. “Generalized Theorems for Nonlinear State Space Reconstruction”. In: *PLOS ONE* 6.3 (Mar. 2011), pp. 1–8. DOI: 10.1371/journal.pone.0018295. URL: <https://doi.org/10.1371/journal.pone.0018295>.
- [10] Tim Sauer, James A. Yorke, and Martin Casdagli. “Embedology”. In: *Journal of Statistical Physics* 65.3 (1991), pp. 579–616. ISSN: 1572-9613. DOI: 10.1007/BF01053745. URL: <https://doi.org/10.1007/BF01053745>.
- [11] E.N. Lorenz. “Predictability: a problem partly solved”. In: *Seminar on Predictability, 4-8 September 1995*. Vol. 1. ECMWF. Shinfield Park, Reading: ECMWF, 1995, pp. 1–18. URL: <https://www.ecmwf.int/node/10829>.
- [12] Z.-M. Chen, K. Djidjeli, and W.G. Price. “Computing Lyapunov exponents based on the solution expression of the variational system”. In: *Applied Mathematics and Computation* 174.2 (2006), pp. 982–996. ISSN: 0096-3003. DOI: <https://doi.org/10.1016/j.amc.2005.05.016>. URL: <https://www.sciencedirect.com/science/article/pii/S0096300305005254>.
- [13] Ethan Deyle et al. “Tracking and forecasting ecosystem interactions in real time”. In: *Proceedings of the Royal Society B: Biological Sciences* 283 (Jan. 2016), p. 20152258. DOI: 10.1098/rspb.2015.2258.
- [14] Konstantinos E. Chlouverakis and J.C. Sprott. “A comparison of correlation and Lyapunov dimensions”. In: *Physica D: Nonlinear Phenomena* 200.1 (2005), pp. 156–164. ISSN: 0167-2789. DOI: <https://doi.org/10.1016/j.physd.2004.10.006>. URL: <https://www.sciencedirect.com/science/article/pii/S0167278904004038>.

- [15] Peter Grassberger and Itamar Procaccia. “Characterization of Strange Attractors”. In: *Phys. Rev. Lett.* 50 (5 1983), pp. 346–349. DOI: 10.1103/PhysRevLett.50.346. URL: <https://link.aps.org/doi/10.1103/PhysRevLett.50.346>.
- [16] Michael D. Hartl. “Lyapunov exponents in constrained and unconstrained ordinary differential equations”. In: *arXiv: Computational Physics* (2003).
- [17] *Wormatlas*. <https://www.wormatlas.org>. Accessed: 2022-12-21.
- [18] Pierre Gaspard and Xiao-Jing Wang. “Noise, chaos, and (ϵ , τ)-entropy per unit time”. In: *Physics Reports* 235.6 (1993), pp. 291–343. ISSN: 0370-1573. DOI: [https://doi.org/10.1016/0370-1573\(93\)90012-3](https://doi.org/10.1016/0370-1573(93)90012-3). URL: <https://www.sciencedirect.com/science/article/pii/0370157393900123>.
- [19] Rainer Engelken, Fred Wolf, and L. F. Abbott. *Lyapunov spectra of chaotic recurrent neural networks*. 2020. DOI: 10.48550/ARXIV.2006.02427. URL: <https://arxiv.org/abs/2006.02427>.

8 Appendix

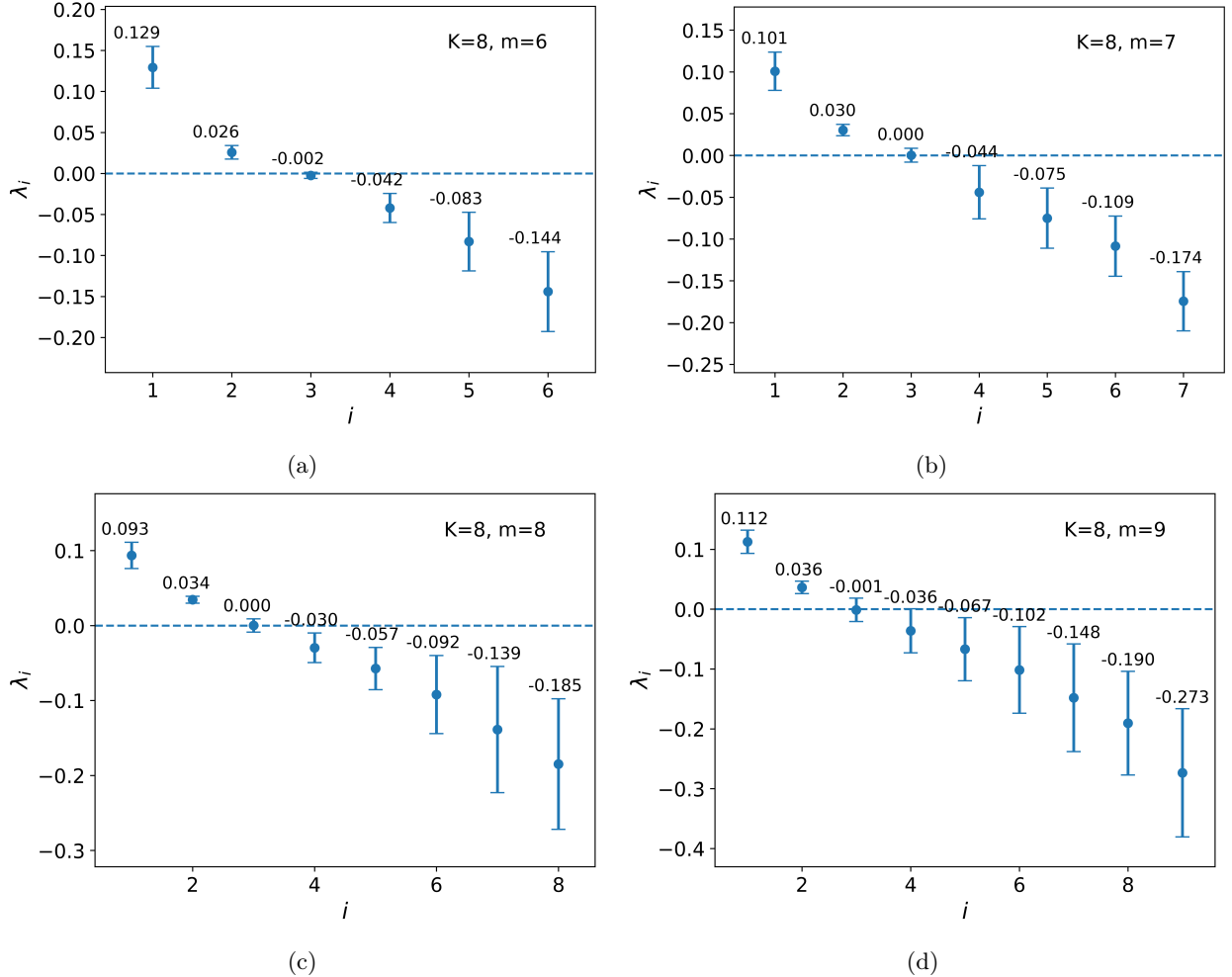


Figure 11: Lyapunov exponents computed from calcium imaging data of *C. Elegans* for $K = 8$ and $m = 6$ (a), 7 (b), 8 (c), 9 (d). The given values correspond to the computed Lyapunov exponent.